STIM1 and calmodulin interact with Orai1 to induce Ca²⁺-dependent inactivation of CRAC channels

Franklin M. Mullins[a,b,1], Chan Young Park[c,1], Ricardo E. Dolmetsch[c,2], and Richard S. Lewis[b,2]

Departments of [a]Pathology, [b]Molecular and Cellular Physiology, and [c]Neurobiology, Stanford University School of Medicine, Stanford, CA 94305

Ca²⁺-dependent inactivation (CDI) is a key regulator and hallmark of the Ca²⁺ release-activated Ca²⁺ (CRAC) channel, a prototypic store-operated Ca²⁺ channel. Although the roles of the endoplasmic reticulum Ca²⁺ sensor STIM1 and the channel subunit Orai1 in CRAC channel activation are becoming well understood, the molecular basis of CDI remains unclear. Recently, we defined a minimal CRAC activation domain (CAD; residues 342–448) that binds directly to Orai1 to activate the channel. Surprisingly, CAD-induced CRAC currents lack fast inactivation, revealing a critical role for STIM1 in this gating process. Through truncations of full-length STIM1, we identified a short domain (residues 470–491) C-terminal to CAD that is required for CDI. This domain contains a cluster of 7 acidic amino acids between residues 475 and 483. Neutralization of aspartate or glutamate pairs in this region either reduced or enhanced CDI, whereas the combined neutralization of six acidic residues eliminated inactivation entirely. Based on bioinformatics predictions of a calmodulin (CaM) binding site on Orai1, we also investigated a role for CaM in CDI. We identified a membrane-proximal N-terminal domain of Orai1 (residues 68–91) that binds CaM in a Ca²⁺-dependent manner and mutations that eliminate CaM binding abrogate CDI. These studies identify novel structural elements of STIM1 and Orai1 that are required for CDI and support a model in which CaM acts in concert with STIM1 and the N terminus of Orai1 to evoke rapid CRAC channel inactivation.

calcium | ion channel gating | store-operated calcium entry | patch-clamp | calcium-binding proteins

Store-operated Ca²⁺ channels provide a major route for receptor-stimulated Ca²⁺ entry in nonexcitable cells (1). The Ca²⁺-release activated Ca²⁺ (CRAC) channel, the best-characterized store-operated channel, is essential for generating Ca²⁺ signals that drive the activation of T lymphocytes, mast cells, and platelets (2–4). CRAC channel activity is shaped by the combination of store-dependent activation and Ca²⁺-dependent inactivation (CDI) processes. The mechanisms linking depletion of Ca²⁺ from the endoplasmic reticulum (ER) to activation of the CRAC channel are becoming well understood: reduction of ER luminal Ca²⁺ causes the ER Ca²⁺ sensor STIM1 (5, 6) to oligomerize (7), enabling its accumulation at ER-plasma membrane junctions (3, 8, 9), where it binds directly to the CRAC channel subunit Orai1 (10–12) to open the channel (13, 14).

Compared with activation, much less is known about the mechanisms underlying CDI, one of the hallmark characteristics of the CRAC current (I_{CRAC}) in mammalian cells. Initial studies in mast cells and T cells revealed that Ca²⁺ influx at hyperpolarized potentials drives rapid inactivation on a time scale of tens of milliseconds through the binding of Ca²⁺ to sites located several nanometers from the intracellular mouth of the pore (15, 16). Subsequent studies have suggested that calmodulin (CaM) and STIM1 both may contribute to this process. In a rat liver cell line, overexpression of a Ca²⁺-insensitive CaM mutant or a CaM inhibitory peptide modestly inhibited fast inactivation of a CRAC-like current (17), suggesting that CaM may promote CDI of the CRAC channel in a manner analogous to its well-established role in the inactivation of voltage-gated Ca²⁺ channels (18, 19). Also, CRAC channels fail to display CDI when they

are activated by a minimal soluble fragment of STIM1 [amino acids 342–448, known as the CRAC activation domain (CAD)], revealing a critical role for STIM1 in CDI (13). Consistent with such a role, a recent report showing that the extent of inactivation correlates with the STIM1/Orai1 transfection ratio further suggests that the number of STIM1 proteins bound to a CRAC channel influences its ability to inactivate (20). Another recent study identified a STIM1 domain (amino acids 475–485) that reduces CRAC channel activity, but its effect on CDI was not examined (21).

In this study, we address the roles of STIM1 and CaM in the CDI of CRAC channels. Using a combination of serial truncations and mutagenesis, we identify a negatively charged region of STIM1 that is required for inactivation. We also identify a region in the N terminus of Orai1 that binds CaM in a Ca²⁺-dependent manner and demonstrate that CaM binding is required for CDI to occur. These results reveal the structural underpinnings of CRAC channel inactivation, identify Orai1 as a CaM-binding protein, and extend the known roles of STIM1 from those of Ca²⁺ sensor and activating ligand to that of a CRAC channel subunit that controls inactivation gating in response to local Ca²⁺ accumulation.

Results

CDI of Heterologously Expressed CRAC Channels. In HEK293 cells transfected with STIM1 and Orai1 at a 1:1 mass ratio, the CRAC current (I_{CRAC}) evoked by EGTA in the recording pipette inactivated rapidly during 200-ms hyperpolarizations to potentials of −60 to −120 mV (Fig. 1A). Similar to native I_{CRAC} in Jurkat T cells (16), inactivation in transfected HEK cells was greatly enhanced in 20 mM Ca²⁺ₒ relative to 2 mM Ca²⁺ₒ, and followed a biexponential time course with time constants of ≈10 and ≈100 ms (Fig. S1). These similarities were apparent despite I_{CRAC} densities >20-fold greater than those of untransfected Jurkat cells (Fig. S2), consistent with previous evidence that rapid CDI is a local process that is driven by Ca²⁺ binding to sites located within nanometers of the inner pore mouth (16).

A Short Domain of STIM1 C-Terminal to CAD Is Required for CDI. CRAC channels can be activated independently of store depletion by direct binding of a minimal peptide derived from the cytoplasmic region of STIM1 (CAD, amino acids 342–448; also called SOAR, amino acids 344–442) (13, 14). Surprisingly, when I_{CRAC} was activated in this way, the current failed to inactivate (Fig. 1B) (13), suggesting that elements of STIM1 outside CAD are necessary for CDI. At very hyperpolarized potentials (−120
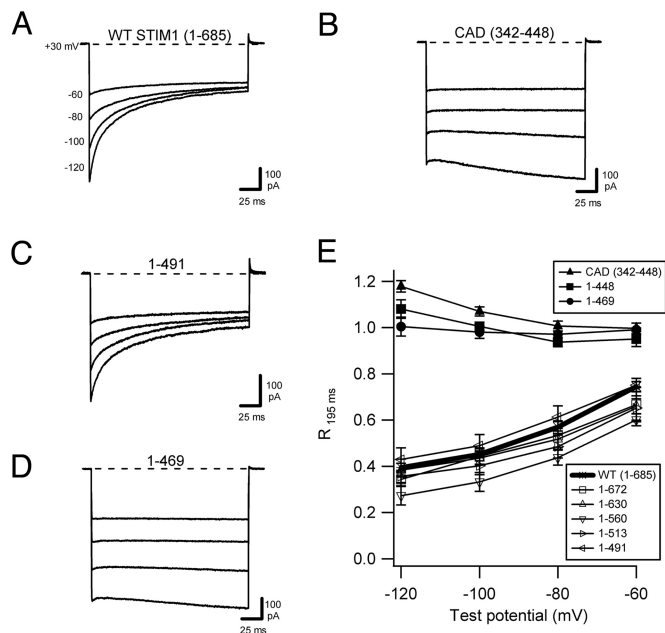
PHYSIOLOGY

Fig. 1. Identification of a STIM1 domain required for rapid CDI of the CRAC channel. All currents were recorded in HEK293 cells cotransfected with myc-Orai1 and the indicated STIM1-derived construct after induction of I_{CRAC} reached a maximum ($\approx$300 s for STIM1, >100 s for CAD). (A–D) Representative currents recorded in 20 mM Ca^{2+}_o during pulses to the voltages indicated for WT GFP-STIM1$_{1-685}$ (A), YFP-CAD (STIM1$_{342-448}$) (B), GFP-STIM1$_{1-491}$ (C), and GFP-STIM1$_{1-469}$ (D). (E) Extent of inactivation, quantified as R$_{195 ms}$, the residual current remaining at the end of the test pulse at 195 ms relative to the peak current at 3 ms, plotted against test potential. mCherry-STIM1$_{1-672}$, GFP-STIM1$_{1-630}$, GFP-STIM1$_{1-560}$, GFP-STIM1$_{1-513}$, and GFP-STIM1$_{1-491}$ inactivate to a similar extent as WT GFP-STIM1, whereas YFP-CAD, mCherry-STIM1$_{1-448}$, and GFP-STIM1$_{1-469}$ fail to inactivate. Each point represents the mean ± SEM of five to eight cells.

mV), CAD-induced I_{CRAC} increased slightly during the voltage step. This behavior varied from cell to cell and was also observed for several other noninactivating constructs described below, but it was not studied further. To identify elements of STIM1 required for CDI, we examined I_{CRAC} in cells coexpressing Orai1 and a series of STIM1 proteins truncated at locations downstream of the CAD. Deletion of residues from amino acid 491 to the STIM1 C terminus did not affect CDI (Fig. 1 C and E), clearly demonstrating that the serine/proline-rich and polybasic domains of STIM1 are dispensable with respect to fast inactivation. However, further shortening of STIM1 (amino acids 1–469 and 1–448) completely prevented CDI (Fig. 1 D and E). Together, these results identify amino acids 470–491 as a functional domain of STIM1 required for fast inactivation of the human CRAC channel. For convenience, we refer to this region hereafter as the inactivation domain of STIM or ID$_{STIM}$.

We next tested whether the ID$_{STIM}$ could restore inactivation to CRAC channels activated by soluble CAD-containing peptides. As expected from the results with truncated STIM1 in Fig. 1, extensions of CAD N-terminally to the ER membrane (STIM1$_{234-448}$) or C-terminally to the start of ID$_{STIM}$ (STIM1$_{342-469}$) failed to restore CDI (Fig. S3 A and B). Interestingly, however, C-terminal extensions of the soluble CAD peptide that included ID$_{STIM}$ only partially restored CDI. The extended peptides STIM1$_{342-560}$ and STIMI$_{342-630}$ supported approximately half the extent of inactivation observed with analogous constructs containing the additional regions N-terminal to CAD (i.e., STIM1$_{1-560}$ and STIMI$_{1-630}$) (Fig. S3 C–E). Thus, ER-bound forms of STIM1 appear to inactivate CRAC channels more efficiently than soluble forms (see Discussion).
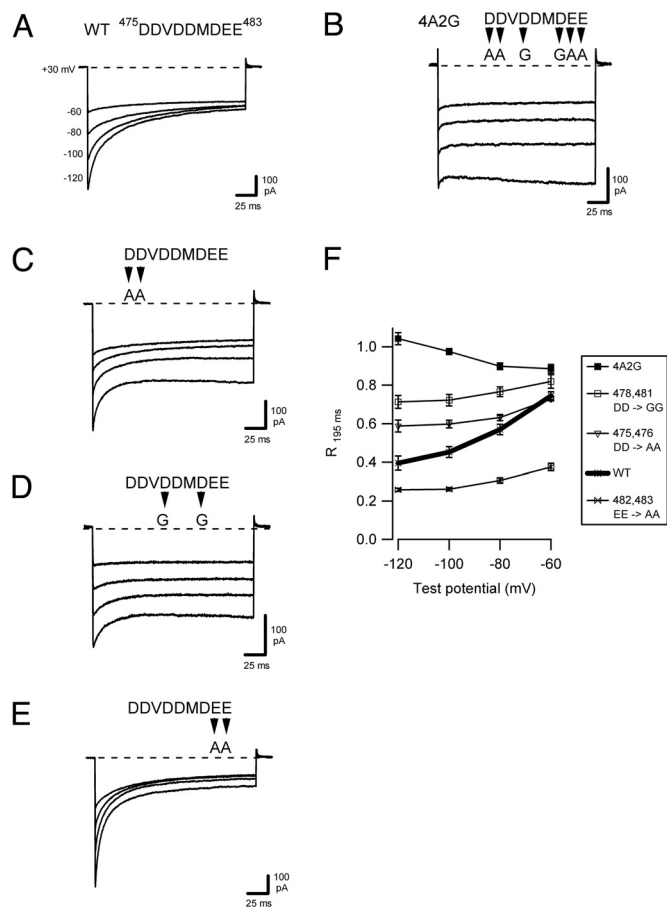

Fig. 2. Neutralization of conserved acidic residues in the inactivation domain of STIM1 alters fast inactivation. All currents were recorded as described in Fig. 1. Mutations introduced between positions 475 and 483 are indicated. (A–E) Representative currents recorded in 20 mM Ca^{2+}_o during pulses to the voltages indicated for WT GFP-STIM1 (1–685, reproduced from Fig. 1 A) (A), myc-STIM1 4A2G (B), GFP-STIM1 (475/476 DD → AA) (C), myc-STIM1 (478/481 DD → GG) (D), and GFP-STIM1 (482/483 EE → AA) (E). (F) The extent of inactivation for each of the STIM1 variants in A–E, quantified as in Fig. 1, and plotted against test potential. Each point represents the mean ± SEM of 5–10 cells.

Neutralization of Conserved Acidic Residues Within ID$_{STIM}$ Affects CDI.
A distinctive feature of the ID$_{STIM}$ is a cluster of 7 acidic residues between amino acids 475 and 483 (DDVDDMDEE; Fig. S4A). To test for a role of these residues in CDI, we introduced mutations in this region. Neutralization of six of the acidic residues in full-length STIM1 completely prevented CDI, consistent with a critical function in mediating inactivation (4A2G; Fig. 2B). More subtle mutations altered the extent and kinetics of CDI. Neutralization of amino acids 475, 476 (DD → AA) or 478, 481 (DD → GG) reduced the extent of CDI (Fig. 2 C, D, and F), whereas neutralization of amino acids 482, 483 (EE → AA) enhanced inactivation relative to WT STIM1 (Fig. 2 E, and F). Interestingly, the EE → AA mutant in 2 mM Ca^{2+}_o inactivated to a similar extent as the WT STIM1 in 20 mM Ca^{2+}_o (Fig. S5), suggesting that the mutations increased the Ca^{2+} sensitivity of CDI. In sum, these results indicate that the acidic residues between amino acids 475 and 483 are critical determinants of CRAC channel CDI, and that both charge and position contribute to their function.

The importance of the negative charges in the ID$_{STIM}$ for CDI raised the possibility that this region may form a binding site for Ca^{2+}. We tested for Ca^{2+} binding by performing $^{45}Ca^{2+}$ overlay experiments with WT and mutant STIM1 polypeptides (Fig. S6).
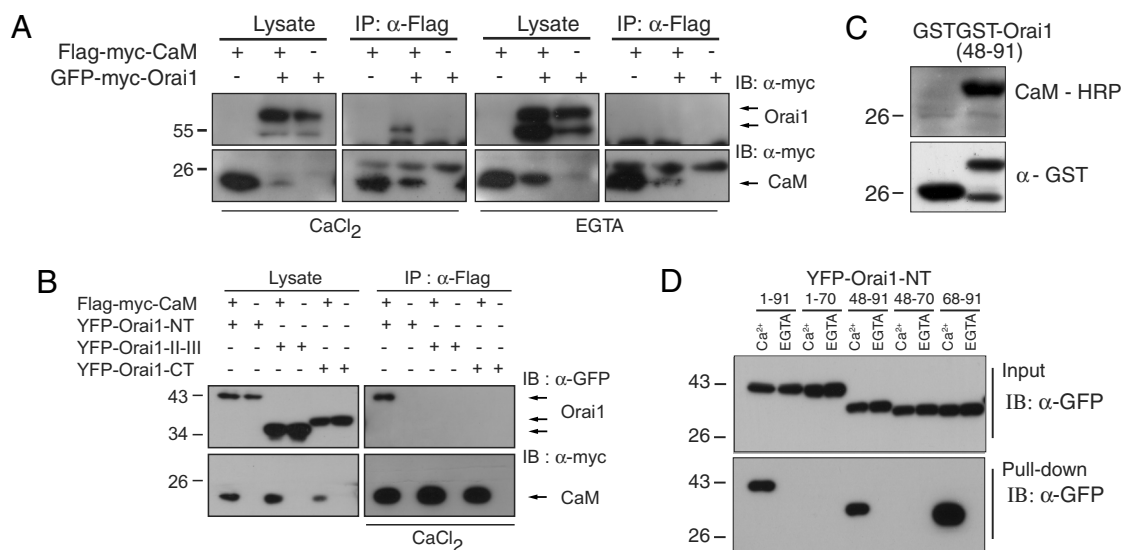
Fig. 3. Ca^{2+}–CaM binds to the membrane-proximal N terminus of Orai1. (*A*) Ca^{2+}-dependent interaction of CaM with full-length Orai1. Flag-myc-CaM and GFP-myc-Orai1 were expressed as indicated in HEK 293T cells. An anti-Flag antibody coimmunoprecipitated GFP-myc-Orai1 with Flag-myc-CaM in the presence of Ca^{2+} (2 mM $CaCl_2$; *Left*), but not under Ca^{2+}-free conditions (4 mM EGTA; *Right*). (*B*) CaM interacts specifically with the Orai1 N terminus. Flag-myc-CaM coimmunoprecipitated with YFP-tagged Orai1 N terminus (amino acids 1–91), but not with the II–III loop (amino acids 142–177) or C terminus (amino acids 255–301) of Orai1. (*C*) CaM–HRP overlay in the presence of Ca^{2+} demonstrating a direct interaction between GST-Orai1$_{48-91}$ and CaM–HRP. CaM–HRP did not interact with GST (at left). (*D*) CaM Sepharose pull-down indicates Ca^{2+}-dependent binding of CaM to amino acids 68–91 of Orai1. The indicated fragments derived from the Orai1 N terminus were expressed and lysates were applied to CaM-Sepharose in the presence of Ca^{2+} or EGTA. All constructs containing amino acids 68–91 of Orai1 bound to CaM in a Ca^{2+}-dependent manner.

$^{45}Ca^{2+}$ binding to WT STIM1 peptide and the DD → AA, DD → GG, and the 4A2G mutant peptides approximately paralleled the degree of CDI observed for each corresponding full-length STIM1 construct; however, binding to WT STIM1 peptide was significantly weaker than binding to CaM. Also, the EE → AA mutant bound $^{45}Ca^{2+}$ less avidly than WT peptide, in contrast to its ability to increase the Ca^{2+} sensitivity of CDI (Fig. S5). The low affinity of Ca^{2+} binding and its inconsistent correlation with CDI call into question whether ID_{STIM} serves as a Ca^{2+} sensor for CDI.

CaM Binding Domain in the Membrane-Proximal Orai1 N Terminus. Given that the physiological role of ID_{STIM} as a Ca^{2+}-binding domain is uncertain, we examined a possible function for CaM in CDI. A previous study of a hepatocyte cell line suggested that CaM contributes to I_{CRAC} inactivation, although its site of action was unknown (17). CaM has also been shown to bind in vitro to the extreme C-terminal polybasic domain of STIM1, and on this basis, a role in control of STIM–Orai complexes was proposed (22). However, we observed that this region is not required for CDI (Fig. 1 *C* and *E*). Bioinformatics analysis predicts a CaM binding site at amino acids 70–87 in the N terminus of Orai1 (4, 23). To test whether CaM binds to Orai1, we coexpressed Flag-myc-CaM and GFP-myc-Orai1 in HEK293T cells and immunoprecipitated CaM using anti-Flag antibodies (Fig. 3*A*). GFP-myc-Orai1 coimmunoprecipitated with Flag-myc-CaM efficiently only in the presence of Ca^{2+} in the lysis buffer, suggesting that Orai1 interacts with CaM in a Ca^{2+}-dependent manner. We mapped the CaM interaction domain of Orai1 by coexpressing Flag-myc-CaM with either the N terminus, the C terminus, or the II–III intracellular loop of Orai1 and immunoprecipitating CaM (Fig. 3*B*). CaM associated only with the N terminus of Orai1. Parallel experiments, in which Orai1 fragments were precipitated by CaM-Sepharose, showed that CaM interaction with the N terminus is Ca^{2+}-dependent (Fig. S7). To refine the location of the binding region within the Orai1 N terminus, we first applied a CaM overlay assay to an Orai1

N-terminal peptide (amino acids 48–91). Horseradish peroxidase-coupled CaM was seen to bind the peptide in the presence of Ca^{2+}, indicating a direct interaction of the two proteins (Fig. 3*C*). CaM-Sepharose pull-down assays using various Orai1 fragments further narrowed the interaction site for Ca^{2+}–CaM to amino acids 68–91, which overlaps with the predicted location of the CaM binding site (Figs. 3*D* and 4*A*). Together, these results show that CaM binds in a Ca^{2+}-dependent manner to a 24-aa CaM binding domain in the N terminus of Orai1 (amino acids 68–91; CBD_{Orai}).

Mutations That Eliminate CaM Binding to CBD_{Orai} also Prevent CDI. We next introduced mutations in Orai1 that interfere with CaM binding to test whether Ca^{2+}–CaM binding is required for I_{CRAC} inactivation. Because CaM often interacts with the hydrophobic surface of amphipathic helices (24), a helical wheel was used to identify hydrophobic residues on one face of CBD_{Orai} (Fig. 4*A*). We generated seven CBD_{Orai} mutations at residues A73, W76, and Y80 in Orai1 N-terminal peptides (amino acids 1–91) and measured their effects on binding to CaM by using a modified CaM-Sepharose pull-down assay. The assay included a WT Orai1-GFP peptide that could be distinguished from the mutants based on size and allowed internal comparisons with the extent of CaM binding by WT Orai1. Five mutations (A73E, W76A, W76E, W76S, and Y80E) abolished CaM binding, whereas two other mutations (Y80A and Y80S) retained binding (Fig. 4*A*). To assess their effects on inactivation, identical point mutations were made in full-length Orai1, which was then coexpressed with STIM1 in HEK293 cells. All five mutations that disrupted CaM binding blocked inactivation of I_{CRAC} (Fig. 4 *C–G*), whereas the two mutations that retained CaM binding yielded strong CDI with accelerated kinetics, consistent with allosteric effects on the inactivation transition (Fig. 4 *H* and *I* and Fig. S8). The consistent correlation between CaM binding and CDI strongly suggests that Ca^{2+}–CaM binding to the N terminus of Orai1 is required for I_{CRAC} inactivation.

Fig. 4. Orai1 mutations that prevent CaM binding also block inactivation. (*A*) Effects of Orai1 mutations on CaM binding. The predicted CaM binding site is shown in bold within the amino acids 68–91 region of Orai1. A73, Y80, and W76 are shown in bold on the predicted hydrophobic face of a helical wheel projection. For the CaM-Sepharose pull-down of WT and mutant Orai1$_{1-91}$ peptides, each lane contains WT peptide and the mutant indicated above. Of the mutant peptides, only Y80A and Y80S retained CaM binding ability. (*B–I*) Representative currents recorded in 20 mM Ca^{2+}o during pulses to the indicated voltages for WT myc-Orai1 (traces reproduced from Fig. 1*A*) (*B*), myc-Orai1 A73E (*C*), myc-Orai1 W76E (*D*), myc-Orai1 W76A (*E*), myc-Orai1 W76S (*F*), myc-Orai1 Y80E (*G*), myc-Orai1 Y80A (*H*), and myc-Orai1 Y80S (*I*). All cells were cotransfected with WT GFP-STIM1$_{1-685}$. (*J*) Extent of inactivation, quantified as the residual current remaining at the end of the test pulse ($R_{195 ms} = I_{195 ms}/I_{1.5 ms}$), plotted against test potential. Peak currents were measured at 1.5 rather than 3 ms because of the rapid inactivation kinetics of Orai1 Y80A and Y80S (Fig. S8). Each point shows the mean ± SEM of five to six cells.

Discussion

Our results show that interactions of STIM1 and CaM with Orai1 underlie rapid CDI of the CRAC channel. Based on early observations that only fast Ca^{2+} buffers like 1,2-bis(2-aminophenoxy)ethane-*N,N,N′,N′*-tetraacetic acid (BAPTA) can bind Ca^{2+} quickly enough to reduce CDI of I_{CRAC} (15, 16), a simple diffusion model predicted that at least two Ca^{2+} ions must bind within several nanometers of the pore to drive inactivation (16). Our results now reveal that Ca^{2+}–CaM binds to Orai1 immediately adjacent to the plasma membrane and therefore may provide Ca^{2+} binding sites required for CDI. It is unclear whether Ca^{2+} binding to the cluster of negative charges in ID$_{STIM}$ is also involved.

A role in CDI significantly extends the functions of STIM1 and its relationship to the CRAC channel. STIM1 is now well established as an ER Ca^{2+} sensor for CRAC channel activation (5, 6, 9, 25) and as a ligand that binds directly to Orai1 to open the channel (13, 14). The finding that a part of STIM1 (the ID$_{STIM}$) is required for the CRAC channel to respond to an extrinsic ligand (Ca^{2+}) shows that STIM1 also acts as a functional subunit of the channel by associating with the pore-forming subunit Orai1 to enable inactivation.

Sequence variation in the regions of STIM1 and Orai1 that are required for CDI may help explain species-specific differences in I_{CRAC} inactivation. The ID$_{STIM}$ is identical among vertebrates, including human, rat, and mouse, in which I_{CRAC} is known to

inactivate (15, 26), but is not well conserved among invertebrates like *Drosophila melanogaster* and *Caenorhabditis elegans*, in which inactivation is absent (Fig. S4*A*) (27, 28). Likewise, the CBD$_{Orai}$ is identical among human, rat, and mouse, but varies in *Drosophila* and *C. elegans* Orai at key residues (A73, W76, and Y80) that we have shown to be critical for CaM binding and CDI in human Orai1 (Fig. 4 and Fig. S4*B*). Mutagenesis and chimera studies will be needed to determine whether these substitutions are sufficient to explain naturally occurring differences in CDI. Also, knocking CDI-deficient variants of Orai1 or STIM1 into mice offers a feasible strategy for determining the physiological role of CDI.

A recent study reported that CRAC channel CDI depends on the expression ratio of STIM1 and Orai1, suggesting that inactivation increases with the number of STIM1s bound to the channel (20). We considered the possibility that the lack of inactivation in our experiments might have resulted from inefficient expression of some STIM1 mutants leading to a low STIM1/Orai1 coupling ratio. However, increasing the STIM1/Orai1 transfection ratio from 1:1 to 4:1 had no discernable effect on the CDI of STIM1$_{1-469}$ or STIM1$_{4A2G}$ (Fig. S9). Thus, specific alterations in STIM1 rather than low coupling ratios are responsible for the absence of inactivation that we observed.

The soluble STIM1 peptides were significantly less effective than their ER-localized counterparts in supporting inactivation (Fig. S3), implying that the architecture of the store-operated Ca^{2+} entry (SOCE) elementary unit itself may have an important role in regulating inactivation. It is relevant to note that the soluble CAD-derived peptides engage and activate CRAC channels throughout the plasma membrane (PM) (13), whereas ER-localized STIM1 forms dense clusters restricted to ER–PM junctions (29). Thus, a likely explanation is that tight clustering at junctions increases the propensity to inactivate, perhaps by increasing the local coupling ratio of STIM/Orai or the local intracellular Ca^{2+} concentration ([Ca^{2+}]$_i$) in the restricted space between the ER and PM. Interestingly, the degree of CDI remains constant as native CRAC channels slowly activate after store depletion (16), suggesting that the coupling stoichiometry and local [Ca^{2+}]$_i$ are also constant or saturating as more channels enter the junctions to become activated.

The identification of ID$_{STIM}$ and the CBD$_{Orai}$ and their roles in CDI are an important step in delineating a molecular mechanism for CDI. Given the rapid kinetics of CDI and the ability of a Ca^{2+}-insensitive CaM to alter inactivation of a CRAC-like current in hepatocytes (17), it is likely that apo-CaM is docked near the channel before Ca^{2+} enters the cell, as is the case for several other types of ion channels (30–32). On channel opening, Ca^{2+} binding to CaM may trigger association with the membrane-proximal CBD$_{Orai}$. This same region of Orai1 is also essential for CRAC channel activation through interactions with the CAD of STIM1 (13). Thus, one hypothesis is that on Ca^{2+} entry Ca^{2+}–CaM displaces the CAD from the N terminus, in effect reversing the activation process to cause CDI. However, such a mechanism seems inconsistent with results of Yamashita et al. (33), who showed that CRAC channels with a pore mutation (E106D) activate normally, but fail to inactivate even with Ca^{2+} as the sole charge carrier. Under those conditions, the CAD is evidently bound even when local [Ca^{2+}]$_i$ is high and Ca^{2+}–CaM would be expected to occupy the CBD$_{Orai}$ site. Although we cannot rule out the possibility that the pore mutation prevents binding of CaM to CBD$_{Orai}$ through an allosteric effect, an alternative mechanism consistent with existing data is that Ca^{2+}-CaM bound to the CBD$_{Orai}$ does not displace the CAD, but instead interacts with the ID$_{STIM}$ region (amino acids 470–491) to drive Orai1 into a nonconducting inactivated state that is available to the WT but not the E106D mutant channel. Further work will be needed to understand in detail the mechanism by which STIM1, CaM, and Orai1 act in concert to evoke rapid inactivation.

Materials and Methods

Cells. HEK293 cells were grown in DMEM with GlutaMax (GIBCO) supplemented with 10% FBS (HyClone) and 1% penicillin/streptomycin (Mediatech) in a humidified, 5% CO$_2$ incubator at 37 °C.

Plasmid cDNA Constructs. N-terminally myc-tagged WT Orai1 (pEX-pGWI-myc-Orai1) has been described (13). This construct was used in all experiments examining the role of STIM1 in CDI. GFP-STIM1 (34), Cherry-STIM1 (29), and YFP-CAD (STIM1$_{342-448}$), YFP-Orai1-NT$_{1-91}$, YFP-Orai1-II-III$_{142-177}$, YFP-Orai1-CT$_{255-301}$, YFP-Orai1$_{1-70}$, YFP-Orai1$_{48-91}$, YFP-Orai1$_{48-70}$, and YFP-Orai1$_{68-91}$ constructs have been described (13).

All primers used for mutagenesis in this study are listed in *SI Text*, and all mutations were confirmed by sequencing. Truncated STIM1 constructs were generated by inserting a stop codon at the appropriate location into the full-length GFP-STIM1 or mCherry-STIM1 construct by QuikChange mutagenesis (Stratagene). For YFP-STIM1$_{234-448}$, YFP-STIM1$_{342-469}$, YFP-STIM1$_{342-560}$, and YFP-STIM1$_{342-630}$, PCR products were cloned into the pCR8/GW/TOPO vector (Invitrogen). Products cloned into this vector were sequenced by using GW1 primer, and Gateway LR clonase reactions (Invitrogen) were used to generate N-terminally YFP-labeled versions using the destination vector pDS-YFP-x (a gift from Tobias Meyer, Stanford University).

Mutations of the conserved negatively charged amino acids between STIM1 positions 475 and 483 were accomplished by QuikChange mutagenesis. N-terminally myc-tagged STIM1 was used as a template for generating myc-STIM1 478, 481 DD → GG. In turn, the myc-STIM1 478, 481 DD → GG construct served as the template for generating the myc-STIM1$_{4A2G}$ construct. GFP-STIM1 475, 476 DD → AA and GFP-STIM1 482, 483 EE → AA were generated by site-directed mutagenesis of the GFP-STIM1 construct.

GFP-Orai1$_{1-91}$ has been described (13). For myc-Orai1-A73E, -W76A, -W76E, -W76S, -Y80A, -Y80E, and -Y80S, N-terminally myc-tagged Orai1 constructs were made by QuikChange mutagenesis. GFP-myc-Orai1$_{1-91}$ was generated by introducing a premature stop codon into GFP-myc-Orai1 by QuikChange. For GFP-myc-Orai1$_{1-91}$-A73E, -W76A, -W76E, -W76S, -Y80A, -Y80E, and -Y80S, QuikChange was applied in the background of GFP-myc-Orai1$_{1-91}$.

CaM was amplified by PCR and cloned into the pCR8 vector. The pDEST-pGW1-Flag-Myc-x vector (custom-designed) was used to generate Flag-Myc-CaM. CaM from pCR8-CaM was excised by NcoI and BamHI digestion and ligated into pET-3d plasmid (Novagen) to generate pET-CaM. CaM (T27C) was constructed by substituting amino acids at residue 27 of CaM (Thr to Cys) by QuikChange.

For GST-Orai1$_{48-91}$, Orai1$_{48-91}$ was excised by BamHI and EcoRI digestion from pCR8-Orai1$_{48-91}$ and ligated into pGEX6p-1.

Transfection. HEK293 cells were transfected with Lipofectamine 2000 (Invitrogen) 8–24 h before electrophysiology experiments. Unless noted otherwise, STIM1- and Orai1-derived constructs were transfected in a 1:1 ratio by mass. For experiments with Cherry-STIM1-derived constructs and STIM1 constructs lacking a fluorophore, eGFP was cotransfected to visualize cells. For experiments with YFP-CAD (STIM1$_{342-448}$) and other STIM1-derived constructs lacking the ER transmembrane domain, cells were incubated in the presence of 10 μM LaCl$_3$ during the interval between transfection and electrophysiology experiments. This treatment served to reduce the toxic effect of constitutively active CRAC current on cells. The fast inactivation phenotype observed for currents induced by YFP-CAD (STIM1$_{342-448}$) in pilot experiments conducted with cells cultured in the absence of 10 μM LaCl$_3$ was identical to that seen when cells were cultured with 10 μM LaCl$_3$.

Recording Solutions. The 2 mM Ca^{2+} extracellular Ringer's solution contained 155 mM NaCl, 4.5 mM KCl, 2 mM CaCl$_2$, 1 mM MgCl$_2$, 10 mM D-glucose, and 5 mM Hepes (pH 7.4 with NaOH). The 20 mM Ca^{2+} extracellular Ringer's solution contained 130 mM NaCl, 4.5 mM KCl, 20 mM CaCl$_2$, 1 mM MgCl$_2$, 10 mM D-glucose, and 5 mM Hepes (pH 7.4 with NaOH). LaCl$_3$ was added directly to parent solutions on the day of the experiment from a 10 mM stock to achieve the desired final concentration. The standard internal solution contained 150 mM Cs aspartate, 8 mM MgCl$_2$, 10 mM EGTA, and 10 mM Hepes (pH 7.2 with CsOH); 10 mM EGTA in the pipette solution does not affect CDI of native CRAC channels (15, 16).

Electrophysiology. Currents were recorded by using the standard whole-cell patch clamp technique as described (13). Cells were patch-clamped at room temperature (22–25 °C) with an Axopatch 200B amplifier (Axon Instruments/

Molecular Devices) interfaced to an ITC-16 input/output board (Instrutech) and a Macintosh G3 computer. Pipettes of resistance 2–5 MΩ were fabricated from 100-μL pipettes (VWR) using a Flaming/Brown puller (model P-87; Sutter Instruments), fire-polished, and coated with Sylgard. Cell and pipette capacitances were nulled before recording. In-house routines developed on the Igor Pro platform (Wavemetrics) were used for stimulation, data acquisition, and analysis. Currents were sampled at 5 kHz and filtered at 2 kHz. Voltages were corrected for the junction potential of the pipette solution relative to Ringer's solution in the bath (-13 mV).

Cells were bathed in 2 mM Ca^{2+} Ringer's solution before seal formation. The holding potential was $+30$ mV. After break-in, cells were pulsed every 5 s with a 100-ms step to -100 mV followed by a 100-ms ramp from -100 to $+100$ mV until current reached a steady-state level (usually 300 s for STIM1 constructs with ER transmembrane domains, which required passive depletion of ER Ca^{2+} stores for current activation). Once a steady state was achieved, the external solution was changed to 20 mM Ca^{2+} Ringer's solution via a multibarrel local perfusion pipette. After the current level during steps to -100 mV had equilibrated to a new steady state in 20 mM Ca^{2+}, a second stimulus protocol consisting of families of 200-ms voltage steps to -60, -80, -100, and -120 mV was applied, with a 5-s interval between steps. Last, both step-ramp and voltage-family protocols were recorded in 20 mM Ca^{2+} Ringer's solution with 10–100 μM $LaCl_3$ for leak subtraction. All summary graphs of current magnitude or functions thereof use leak-subtracted current values.

Data Analysis. Currents from voltage families demonstrating fast inactivation were fit with the biexponential function $I = I_o + A_1 e^{-t/\tau 1} + A_2 e^{-t/\tau 2}$, where $\tau 1$ and $\tau 2$ represent slow and fast time constants of inactivation, respectively. To minimize contributions from uncompensated capacitative current, peak currents were measured at 3 ms after the beginning of the pulse, and biexponential fits of current decay were also started at the 3-ms time point. For Fig. 4, peak currents were measured at the 1.5-ms time point because of the rapid inactivation kinetics of Orai1 Y80A and Y80S. In all cases, steady-state current was measured at the 195-ms time point.

Immunoprecipitation and Immunoblot Analysis. Eighteen hours after transfection, HEK293T cells were washed with PBS twice and lysed in 50 mM Tris·HCl (pH 7.5), 150 mM NaCl, 1% Triton X-100, and protease inhibitors with either 2 mM $CaCl_2$ (for Ca^{2+} condition) or 4 mM EGTA (for Ca^{2+} free condition) for 15 min. Lysates were spun at $13,400 \times g$ for 10 min, and the supernatant was

incubated with anti-Flag M2 agarose beads (Sigma) for 2 h. After washing five times, lysates and immunoprecipitates were subjected to SDS/PAGE and Western blotting analysis.

CaM-HRP Assays. For purified recombinant CaM, pET3-CaM and pET-CaM (T27C) were transformed into *Escherichia coli* BL21 pRIL. Transformants were grown in liquid cultures. IPTG (1 mM) was added at an optical density of $\approx$0.5–0.7 at 600 nm; 3 h after induction at 30 °C, cells were collected by centrifugation and resuspended in extraction buffer [50 mM Tris·HCl (pH 7.5), 2 mM EDTA, 1 mM DTT, and protease inhibitors]. The cell suspensions were sonicated and treated with DNase (1 unit/mL of DNase I and 5 mM $MgCl_2$) for 30 min. After clearing the lysates by centrifugation at $70,714 \times g$ for 30 min at 4 °C, the supernatant was transferred to a new tube and added to 5 mM $CaCl_2$ followed by a denaturation step at 85 °C for 2.5 min. The clear lysate was collected by centrifugation at $7,840 \times g$ for 5 min and applied to phenyl-Sepharose (GE Healthcare) column. After serial washes with binding buffer [30 mM Tris·HCl (pH 7.5), 1 mM $CaCl_2$], washing buffer [30 mM Tris·HCl (pH 7.5), 1 mM $CaCl_2$, 200 mM NaCl], and binding buffer again, recombinant CaMs were eluted with elution buffer [30 mM Tris·HCl (pH 7.5), 2 mM EGTA]. All purified CaMs (CaM and CaM T27C) were dialyzed with 2 mM Tris·HCl, pH 7.5 at 4 °C. Protein concentration was measured by the Bradford method (Bio-Rad).

Conjugation between CaM and HRP was performed as described (35). CaM-HRP gel overlay assays were performed by using crude whole bacterial lysates of GST and GST-Orai1$_{48-91}$ and purified CaM (T27C)-HRP as described (35)

CaM-Sepharose Pull-Down Assay. Transiently transfected HEK293T were lysed in lysis buffer [50 mM Tris·HCl (pH 7.5), 150 mM NaCl, 0.5% Triton X-100, and protease inhibitor with either 2 mM $CaCl_2$ or 4 mM EGTA] for 15 min. After centrifugation, the supernatant was applied to CaM-Sepharose 4B beads (GE Healthcare) for 1 h. After several washes with lysis buffer, SDS loading buffer was added to beads followed by SDS/PAGE.

1. Parekh AB, Putney JW, Jr (2005) Store-operated calcium channels. *Physiol Rev* 85:757–810.
2. Lewis RS (2001) Calcium signaling mechanisms in T lymphocytes. *Annu Rev Immunol* 19:497–521.
3. Varnai P, Hunyady L, Balla T (2009) STIM and Orai: The long-awaited constituents of store-operated calcium entry. *Trends Pharmacol Sci* 30:118–128.
4. Frischauf I, et al. (2008) The STIM/Orai coupling machinery. *Channels* 2:261–268.
5. Liou J, et al. (2005) STIM is a Ca^{2+} sensor essential for Ca^{2+}-store-depletion-triggered Ca^{2+} influx. *Curr Biol* 15:1235–1241.
6. Zhang SL, et al. (2005) STIM1 is a Ca^{2+} sensor that activates CRAC channels and migrates from the Ca^{2+} store to the plasma membrane. *Nature* 437:902–905.
7. Liou J, Fivaz M, Inoue T, Meyer T (2007) Live-cell imaging reveals sequential oligomerization and local plasma membrane targeting of stromal interaction molecule 1 after Ca^{2+} store depletion. *Proc Natl Acad Sci USA* 104:9301–9306.
8. Wu MM, Luik RM, Lewis RS (2007) Some assembly required: Constructing the elementary units of store-operated Ca^{2+} entry. *Cell Calcium* 42:163–172.
9. Luik RM, Wang B, Prakriya M, Wu MM, Lewis RS (2008) Oligomerization of STIM1 couples ER calcium depletion to CRAC channel activation. *Nature* 454:538–542.
10. Prakriya M, et al. (2006) Orai1 is an essential pore subunit of the CRAC channel. *Nature* 443:230–233.
11. Yeromin AV, et al. (2006) Molecular identification of the CRAC channel by altered ion selectivity in a mutant of Orai. *Nature* 443:226–229.
12. Vig M, et al. (2006) CRACM1 multimers form the ion-selective pore of the CRAC channel. *Curr Biol* 16:2073–2079.
13. Park CY, et al. (2009) STIM1 clusters and activates CRAC channels via direct binding of a cytosolic domain to Orai1. *Cell* 136:876–890.
14. Yuan JP, et al. (2009) SOAR and the polybasic STIM1 domains gate and regulate Orai channels. *Nat Cell Biol* 11:337–343.
15. Hoth M, Penner R (1993) Calcium release-activated calcium current in rat mast cells. *J Physiol (London)* 465:359–386.
16. Zweifach A, Lewis RS (1995) Rapid inactivation of depletion-activated calcium current (I_{CRAC}) due to local calcium feedback. *J Gen Physiol* 105:209–226.
17. Litjens T, Harland ML, Roberts ML, Barritt GJ, Rychkov GY (2004) Fast Ca^{2+}-dependent inactivation of the store-operated Ca^{2+} current (I_{SOC}) in liver cells: A role for calmodulin. *J Physiol (London)* 558:85–97.
18. Levitan IB (1999) It is calmodulin after all! Mediator of the calcium modulation of multiple ion channels. *Neuron* 22:645–648.
19. Saimi Y, Kung C (2002) Calmodulin as an ion channel subunit. *Annu Rev Physiol* 64:289–311.
20. Scrimgeour N, Litjens T, Ma L, Barritt GJ, Rychkov GY (2009) Properties of Orai1 mediated store-operated current depend on the expression levels of STIM1 and Orai1 proteins. *J Physiol (London)* 587:2903–2918.
21. Muik M, et al. (2009) A cytosolic homomerization and a modulatory domain within STIM1 C terminus determine coupling to ORAI1 channels. *J Biol Chem* 284:8421–8426.
22. Bauer MC, O'Connell D, Cahill DJ, Linse S (2008) Calmodulin binding to the polybasic C termini of STIM proteins involved in store-operated calcium entry. *Biochemistry* 47:6089–6091.
23. Yap KL, et al. (2000) Calmodulin target database. *J Struct Funct Genomics* 1:8–14.
24. O'Neil KT, DeGrado WF (1990) How calmodulin binds its targets: Sequence independent recognition of amphiphilic α-helices. *Trends Biochem Sci* 15:59–64.
25. Stathopulos PB, Zheng L, Li GY, Plevin MJ, Ikura M (2008) Structural and mechanistic insights into STIM1-mediated initiation of store-operated calcium entry. *Cell* 135:110–122.
26. Oh-Hora M, et al. (2008) Dual functions for the endoplasmic reticulum calcium sensors STIM1 and STIM2 in T cell activation and tolerance. *Nat Immunol* 9:432–443.
27. Yeromin AV, Roos J, Stauderman KA, Cahalan MD (2004) A store-operated calcium channel in *Drosophila* S2 cells. *J Gen Physiol* 123:167–182.
28. Estevez AY, Roberts RK, Strange K (2003) Identification of store-independent and store-operated Ca^{2+} conductances in *Caenorhabditis elegans* intestinal epithelial cells. *J Gen Physiol* 122:207–223.
29. Luik RM, Wu MM, Buchanan J, Lewis RS (2006) The elementary unit of store-operated Ca^{2+} entry: Local activation of CRAC channels by STIM1 at ER-plasma membrane junctions. *J Cell Biol* 174:815–825.
30. Erickson MG, Alseikhan BA, Peterson BZ, Yue DT (2001) Preassociation of calmodulin with voltage-gated Ca^{2+} channels revealed by FRET in single living cells. *Neuron* 31:973–985.
31. Pitt GS, et al. (2001) Molecular basis of calmodulin tethering and Ca^{2+}-dependent inactivation of L-type Ca^{2+} channels. *J Biol Chem* 276:30794–30802.
32. Maylie J, Bond CT, Herson PS, Lee WS, Adelman JP (2004) Small conductance Ca^{2+}-activated K^+ channels and calmodulin. *J Physiol (London)* 554:255–261.
33. Yamashita M, Navarro-Borelly L, McNally BA, Prakriya M (2007) Orai1 mutations alter ion permeation and Ca^{2+}-dependent fast inactivation of CRAC channels: Evidence for coupling of permeation and gating. *J Gen Physiol* 130:525–540.
34. Wu MM, Buchanan J, Luik RM, Lewis RS (2006) Ca^{2+} store depletion causes STIM1 to accumulate in ER regions closely associated with the plasma membrane. *J Cell Biol* 174:803–813.
35. Lee SH, et al. (1999) Competitive binding of calmodulin isoforms to calmodulin-binding proteins: Implication for the function of calmodulin isoforms in plants. *Biochim Biophys Acta* 1433:56–67.